CHEMISTRY OF MATERIALS

ARTICLE

pubs.acs.org/cm

Ferromagnetic Order from p-Electrons in Rubidium Oxide

Syarif Riyadi,[†] Shivakumara Giriyapura,[†] Robert A. de Groot,[†,‡] Antonio Caretta,[†] Paul H. M. van Loosdrecht,[†] Thomas T. M. Palstra,[†] and Graeme R. Blake*[,†]

[†]Zernike Institute for Advanced Materials, University of Groningen, Nijenborgh 4, 9747 AG Groningen, The Netherlands, and [‡]Electronic Structure of Materials, IMM, Radboud University Nijmegen, Toernooiveld 1, 6526 ED Nijmegen, The Netherlands

Supporting Information

ABSTRACT: Magnetic dioxygen molecules can be used as building blocks of model systems to investigate spin-polarization that arises from unpaired p-electrons, the scientific potential of which is evidenced by phenomena such as spin-polarized transport in graphene. In solid elemental oxygen and all of the known ionic salts comprised of magnetic dioxygen anions and alkali metal cations, the dominant magnetic interactions are antiferromagnetic. We have induced novel ferromagnetic interactions by introducing oxygen deficiency in rubidium superoxide (RbO_2). The anion vacancies in the resulting phase with composition $RbO_{1.72}$ provide greater structural flexibility compared to RbO_2 and facilitate a Jahn−Teller-driven order−disorder transition involving the anion orientations at ∼230 K, below which their axes become confined to a plane. This reorganization gives rise to short-range ferromagnetic ordering below ∼50 K. A ferromagnetic cluster-glass state then forms below ∼20 K, embedded in an antiferromagnetic matrix that orders at ∼5 K. We attribute this inhomogeneous magnetic order to either subtly different anion geometries within different structural nanodomains or to the presence of clusters in which double exchange takes place between the anions, which are mixed-valence in nature. We thus demonstrate that nonstoichiometry can be employed as a new route to induce ferromagnetism in alkali metal oxides.

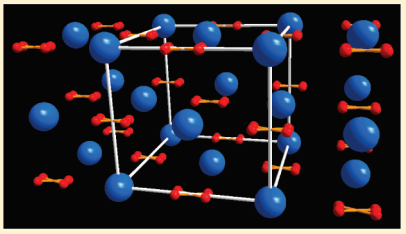

KEYWORDS: ferromagnetism, p-electrons, superoxide, Jahn−Teller, cluster glass

1. INTRODUCTION

Materials whose magnetism arises from main-group elements with unpaired p-electrons have been little explored, largely due to a strong tendency toward electron delocalization and the formation of covalent bonds. Nevertheless, phenomena such as spin-polarized transport in the p-electron system graphene[1,2] demonstrate that such materials may have great scientific and technological potential. A number of "d^0 ferromagnets" have been reported in recent years, some of which have high ordering temperatures.[3−5] In most cases the origin of the magnetism is rather unclear, arising from either defects or low-level chemical doping that apparently induces local moments. Crucially, the magnetic properties of such systems are difficult to control and reproduce. An intuitive approach toward the realization of more concentrated magnetic systems with strong exchange interactions is instead to focus on crystalline solids in which the magnetic entities are spatially ordered and in close proximity.

The best known example of a crystalline p-electron magnetic material is molecular oxygen, which has two unpaired electrons in a doubly degenerate antibonding π_g level. The dioxygen molecule adopts a linear dumbbell shape, the orientation of which in the crystalline state provides an additional degree of freedom when considering the magnetic exchange interactions that are possible. Oxygen possesses an exceedingly rich temperature−pressure phase diagram that includes metallic and superconducting phases as well as a range of antiferromagnetic (AFM) structures.[6] At ambient pressure, solid O_2 exhibits three-dimensional AFM ordering in the α-phase below 24 K.[7] The high-pressure δ-phase adopts three different AFM configurations and magnetic ordering probably exists up to room temperature.[8] The AFM exchange interactions in solid O_2 are attributed to the ubiquitous parallel arrangement of the molecules. However, theory indicates that ferromagnetic (FM) exchange should be realized when adjacent oxygen molecules are orthogonal[9] or "crossed" with respect to each other.[10] Attempts have been made to stabilize this geometry by confining oxygen molecules within nanotubes[11] and organometallic host−guest structures.[12,13]

An alternative route toward manipulating the magnetic exchange interactions of oxygen is to study ionic salts based on dioxygen anions. Molecular oxygen readily accepts one or two electrons from alkali or alkaline earth metals to form the magnetic superoxide and nonmagnetic peroxide anions, with three and four electrons in the π_g level, respectively.[14] The alkali metal superoxides AO_2 all undergo multiple structural phase transitions that involve cooperative tilts and/or shifts of the anions.[15] These transitions are thought to lift the orbital degeneracy of the π_g level that is present at room temperature,[16,17] resulting in probable spatial ordering of the fully occupied and half occupied π_x and π_y orbitals. This is similar to the Jahn−Teller effect in

Received: December 1, 2010
Revised: January 27, 2011
Published: February 22, 2011

transition metal oxides in which orbital order (OO) is induced by shifts of the ligands that surround the orbitally degenerate cation. The magnetic exchange interactions in AO_2 are expected to depend on the resulting interplay between spin, orbital and lattice (orientational) degrees of freedom.[18−22] Although the AO_2 materials adopt a range of different crystal structures, the long-range magnetic ordering that sets in below ∼15 K is always AFM in nature.[15,23]

Here, we study the effect of oxygen deficiency on the properties of AO_2, a parameter that in principle allows control of the π_g level filling via the formation of mixed-valent anion states intermediate to superoxide and peroxide. Although the tuning of mixed valency in transition metal oxides often allows dramatic variation of the physical properties, typified by the doped manganite perovskites,[24] the effect on the properties of the alkali metal oxides has been little explored. We focus on the RbO_{2-x} phase diagram ($x < 1$) in which three phases are currently known: the end members rubidium peroxide (RbO) and superoxide (RbO_2), and the intermediate rubidium sesquioxide ($RbO_{1.5}$). The latter material is mixed-valent and is an insulator that exhibits magnetic frustration below ∼8 K.[25,26] Here we demonstrate that a fourth compound exists in this region of the phase diagram, with composition $RbO_{1.72}$. This material has vacancies on the anion sublattice and exhibits short-range FM ordering below ∼50 K. A FM cluster-glass state forms below ∼20 K, embedded in an AFM matrix that orders at ∼5 K. This inhomogeneous magnetism results either from structural domains with different types of anion ordering or from clusters in which double exchange takes place between the mixed-valence anions.

2. EXPERIMENTAL SECTION

2.1. Synthesis of $RbO_{1.72}$. Polycrystalline rubidium superoxide (RbO_2) was used as a precursor and was prepared by the oxidation of Rb metal dissolved in liquid ammonia at −60 °C. Ammonia was transferred from a compressed gas cylinder through rubber tubing and condensed in an evacuated cooled flask containing Rb metal, where a blue solution was obtained on stirring. Dry oxygen was then flowed through the flask for ∼3 h until the color of the solution became yellow. The ammonia was removed by evaporation while maintaining the oxygen flow, yielding a yellow powder that was revealed by X-ray diffraction (XRD) to contain RbO_2 at a purity of ∼97% together with ∼3% of $RbOH.H_2O$. The RbO_2 precursor was then transferred to a round-bottomed flask that was surrounded by a heating mantle and open to a vacuum line. Pale yellow $RbO_{1.72}$ powder with a cubic crystal structure at room temperature was obtained after heating in a vacuum at 300 °C for 16 h.

2.2. Physical Characterization. Powder X-ray diffraction (XRD) measurements were performed using a Huber G670 diffractometer operating with Cu Kα radiation and a primary monochromator; temperature control was achieved using a closed-cycle refrigerator. Data were collected in the 2θ range 10° to 100° using an imaging plate. Because of the highly hygroscopic nature of the powder, the sample was mounted in a nitrogen-filled glovebox. The powder was sandwiched between two pieces of Mylar film that were clamped in place on the sample holder using a metal ring. After transferal to the diffractometer, the sample chamber was immediately evacuated. Samples mounted under these conditions showed no signs of decomposition on the time scale of the measurements. Data were collected between room temperature and 20 K. The crystal structure was refined using the GSAS software suite in combination with the EXPGUI interface.[27,28] The Xfit software[29] was used to fit selected individual XRD peaks. Magnetization measurements were performed using an MPMS XL-7 SQUID magnetometer. The sample was loaded into a glass NMR tube in a nitrogen-filled glovebox; the tube was then evacuated and sealed before being transferred to the magnetometer. Thermogravimetric analysis (TGA) was carried out in a TA Instruments SDT-400 to determine the oxygen content of the sample by warming to 50 °C in an atmosphere of flowing oxygen that had been passed through a drying column and then measuring the weight gain that occurred on oxidation back to RbO_2. Raman spectroscopy was performed on a sample contained in an evacuated, sealed NMR tube. The sample was excited with a 532 nm laser focused to an area of 50 μm^2. Spectra were measured in a backscattering configuration using a liquid nitrogen-cooled charged coupled device (CCD) connected to a three-grating micro-Raman spectrometer (T64000, Jobin Yvon). Spectra with a resolution of 1.5 cm^{-1} could be obtained using a laser power density of 0.1 mW/μm^2.

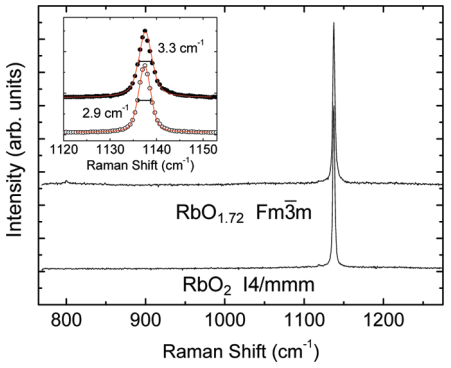

Figure 1. Room-temperature Raman spectra of cubic $RbO_{1.72}$ (top) and tetragonal RbO_2 (bottom). The inset shows an expanded view of the 1138 cm^{-1} peaks with the values of full width at half-maximum indicated.

3. RESULTS

3.1. Chemical Composition. The chemical composition of our sample prepared by thermal decomposition of RbO_2 was determined to be $RbO_{1.72(5)}$ by TGA. The uncertainty in composition arises from difficulty in performing the TGA experiment in a perfectly inert atmosphere; after oxidation back to RbO_2 was complete, the sample continued to gain weight at a slower rate, probably due to trace amounts of water that could not be excluded from the instrument. A second sample prepared using the same protocol had the same composition within experimental uncertainty and essentially identical physical properties. Thermal decomposition with longer heating times and higher temperatures led to formation of the black sesquioxide $RbO_{1.5}$, whereas shorter heating times and lower temperatures did not decompose all of the RbO_2, suggesting that $RbO_{1.72}$ is a line phase.

The oxygen species present in the sample were investigated using Raman spectroscopy. As shown in Figure 1, a peak centered at 1137.6 cm^{-1} is observed for both $RbO_{1.72}$ and the RbO_2 precursor, close to the previously reported O−O stretching mode of the superoxide anion in RbO_2 (1141 cm^{-1}).[15] A weak peak is also present for $RbO_{1.72}$ at 800.6 cm^{-1}, close to the 782 cm^{-1} stretching mode reported for the peroxide anion in RbO.[30] The integrated intensity is 2.5% that of the 1137.6 cm^{-1} peak, consistent with a filling of the π^* level close to that found in the superoxide anion. We note that strong peaks close to both of these positions were observed for $RbO_{1.5}$, which nominally contains two superoxide anions to one peroxide anion.[26] In $RbO_{1.72}$, assuming that the strongly electropositive Rb atom transfers a full electron to the dioxygen molecules, charge balance requires that the π_g orbitals contain 0.84 holes per anion, a mixed-valent

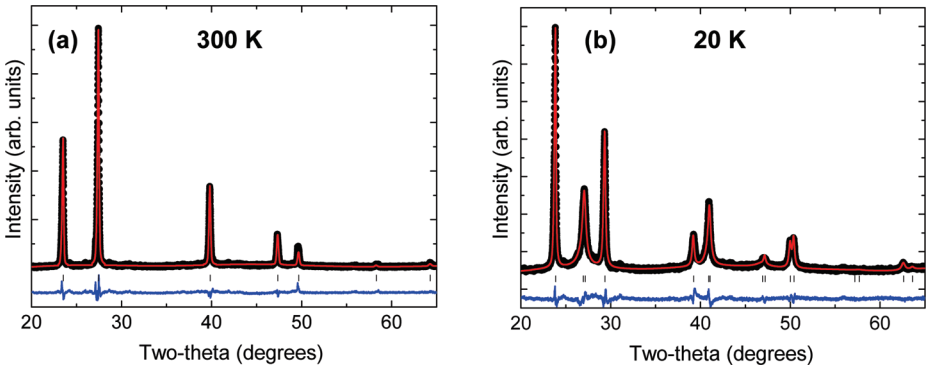

Figure 2. Observed (black), calculated (red), and difference (blue) XRD profiles at (a) 300 and (b) 20 K.

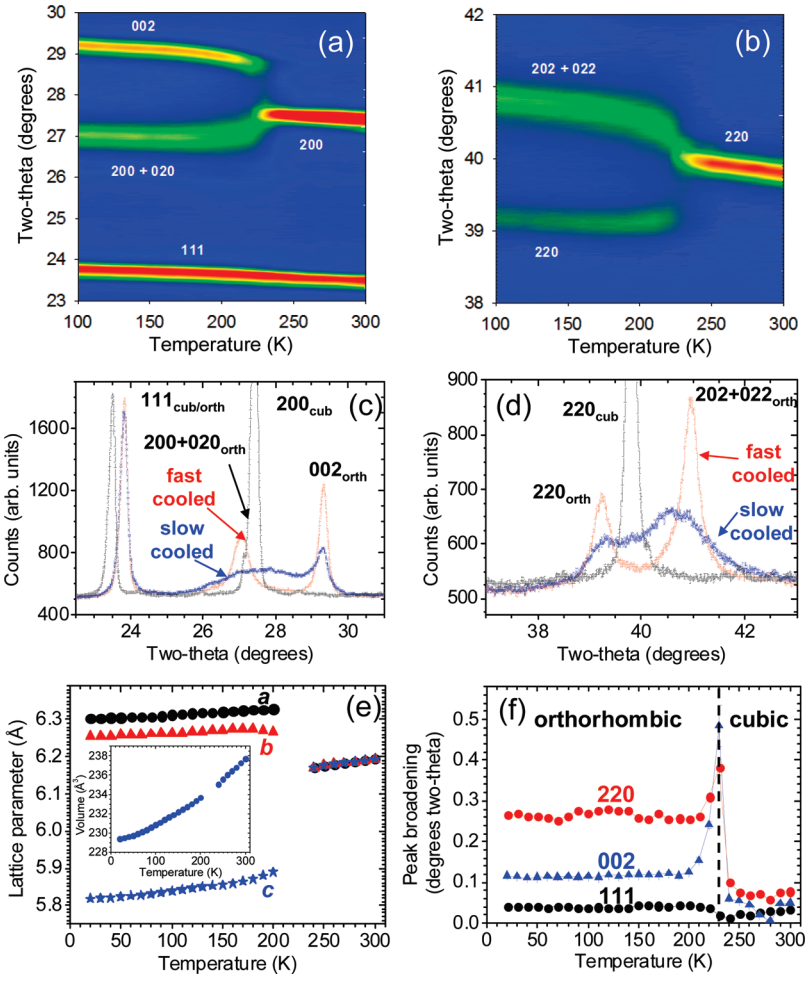

Figure 3. (a, b) Partial XRD patterns of $RbO_{1.72}$ showing the evolution of selected peaks as a function of temperature (color scale shows intensity in arbitrary units). (c, d) Partial XRD patterns collected at 300 K (black) and at 20 K after fast cooling (red) and slow cooling (blue). (e) Evolution of lattice parameters and unit-cell volume with temperature for the fast-cooled sample. (f) Peak broadening (instrumental peak width has been subtracted) of 111, 002, and 220 peaks as a function of temperature for the fast-cooled sample.

situation. The pale yellow color of our sample suggests insulating behavior and hence that the π_g electrons are largely localized, as discussed further in Section 4. The inset to Figure 1 shows fits to the 1137.6 cm^{-1} peak for both the RbO_2 precursor and $RbO_{1.72}$ using pseudo-Voigt functions; the $RbO_{1.72}$ peak is slightly broader, which probably reflects a greater degree of disorder in the local environment of the dioxygen anions. In stoichiometric RbO_2, opposite tilts and shifts of the anions give rise to domains, the coherency of which is broken by stacking faults.[15] In $RbO_{1.72}$, the orientation of the anions is disordered in essentially spherical fashion, as discussed in Section 3.2.

3.2. Crystal Structure. At 300 K, all reflections could be indexed in the cubic $Fm\bar{3}m$ space group with lattice parameter 6.195 Å. Rietveld refinements were carried out using a fixed oxygen site occupancy of 86% to reflect the chemical composition determined by TGA. We note that refinement of the site

dx.doi.org/10.1021/cm103433r |*Chem. Mater.* 2011, 23, 1578–1586

occupancy using the low temperature data sets consistently gave values of 88(1)%; although the site occupancy is strongly correlated with the isotropic displacement factor in the refinements, this value is within experimental uncertainty of the oxygen content determined by TGA. The best fit to the 300 K data (wR_p = 0.0173, see Figure 2a) was obtained using a model with Rb atoms at the origin and dioxygen anions aligned along the four equivalent [111] directions, similar to the room temperature "disordered pyrite" structure of NaO_2.[31] Alternative models in which the anions are aligned along the three equivalent crystal axes (wR_p = 0.0182) and in which they are approximated by a spherical distribution of electron density (wR_p = 0.0191) gave slightly worse fits. We conclude that the anion axes at 300 K have a slight statistical preference for alignment along [111] but exhibit considerable spherical orientational disorder. Despite the good fit, shortcomings in this spatially and time-averaged model were evident from an inability to refine physically meaningful isotropic displacement factors; that of Rb was unreasonably high, and that of O was negative.

On cooling, a phase transition was observed at ~230 K. The cubic 111 (Figure 3a, c) and 222 (not shown) peaks remain single and sharp, whereas the cubic 200 and 220 (Figure 3a−d) peaks split, indicating elongation of two of the cubic crystal axes and shortening of the other. Taking c as the short axis, peaks with hkl, $h \neq k$ are broader than those with $h = k$ below the transition (see for example Figure 3d), suggesting that $a \neq b$. All peaks could be indexed in the orthorhombic space group *Fmmm*. The evolution of the lattice parameters and unit cell volume with temperature is shown in Figure 3e; the sample was cooled to 20 K over ~1.5 h (hereafter referred to as "fast cooled") before diffraction patterns were collected for 1 h each at intervals of 10 K on warming. Between 220 and 240 K the cubic 200 peak coexists with the orthorhombic 002 peak. This, together with the sudden change in lattice parameters between the high and low temperature phases, indirectly suggests that the transition is first-order in nature. However, in the vicinity of the transition all peaks except 111 and 222 are significantly broadened (Figure 3f), preventing the determination of precise lattice parameters for either phase. The phase transition involves orientational ordering of the anions, which become confined to the pseudotetragonal ab plane below ~230 K. In structural refinements of the low-temperature phase it was necessary to introduce a soft constraint to keep the O−O bond length within a realistic range; we constrained it to lie within ~0.02 Å of the expected value of ~1.33 Å for the superoxide anion.[32] The refinements were made more difficult by complex anisotropic peak broadening. Peaks with dominant h and k Miller indices such as 220 were broader than those with dominant l indices such as 002 (Figure 3f). However, the width of the 111 peak remained close to the instrumental resolution at all temperatures. The peak profiles could be modeled reasonably well using the microstrain broadening formalism of Stephens.[33] The refinements suggested that the anions lie with their axes at an angle of ±20° to a (disordered in the *Fmmm* space group), which is consistent with the larger a lattice parameter; the oxygen x and y coordinates are rather strongly correlated with the microstrain broadening parameters in the refinement so this tilt angle has an uncertainty of a few degrees. Difference Fourier plots revealed the presence of electron density around the unit-cell origin where the Rb atoms were initially placed. Consequently, the Rb atoms were moved from the 4*a* site at the origin to the split 16*o* site at (x, y, 0) with fractional occupancy 1/4. A significant improvement in the fit

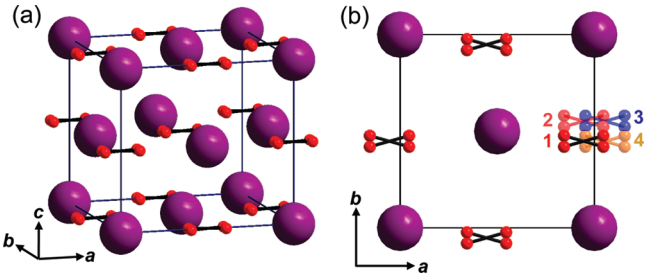

Figure 4. (a) Average crystal structure of $RbO_{1.72}$ at 20 K. (b) Schematic view of *ab* plane showing anion geometry. The anion tilts are disordered in *Fmmm* symmetry. Four pairs of shifted anions labeled 1−4 are shown, giving 8 possible configurations for every site.

Table 1. Refined Crystallographic Parameters for $RbO_{1.72}$ at 20 K in Space Group *Fmmm* with a = 6.3028(3) Å, b = 6.2559(2) Å, c = 5.8180(1) Å[a]

atom	position	x	y	z	occupancy	U_{iso} (Å^2)
Rb	16*o*	0.0548(7)	0.0518(5)	0	0.25	0.0117(7)
O	16*o*	0.399(1)	0.529(3)	0.5	0.43	0.0194(12)

[a] The fractional occupancies were fixed.

was obtained on freely refining the x and y coordinates of this 4-fold split site. The resulting structural model is, in effect, one where Rb lies at the origin of the orthorhombic unit cell and the centers of the anions are shifted by ($\pm xa \pm yb$) from their original positions. Combined with the disordered positive and negative tilts, 8 anion orientations are possible as shown schematically in Figure 4. The refined crystallographic parameters for $RbO_{1.72}$ at 20 K in *Fmmm* symmetry are given in Table 1; the observed, calculated and difference diffraction profiles are shown in Figure 2b (wR_p = 0.0143), and a crystallographic information file (CIF) can be found in the Supporting Information.

The anisotropic peak broadening most likely arises from the presence of microdomains in which the anion shifts and tilts are coherent from cell to cell. The diffraction peaks will be broadened if these domains are small. This picture has previously been used to account for diffuse scattering in single crystal XRD data collected on KO_2.[31] The true symmetry of $RbO_{1.72}$ on a local level would then be noncentrosymmetric and monoclinic at highest; we are unable to probe this further using our powder diffraction data. We note that the relative sharpness of the 111 and 222 peaks suggests a well-defined long-range periodicity in the [111] direction, which implies that the structural domains are strongly elongated.

The diffraction patterns collected on the low-temperature phase depend strongly on the rate at which the sample is cooled through the phase transition. After the first set of diffraction data (fast-cooled) had been collected on warming from 20 K to room temperature, a second set of data was immediately collected at intervals of 10 K on cooling back to 20 K (hereafter referred to as "slow-cooled"). The cubic-to-orthorhombic phase transition gave rise to anisotropic broadening that was much more extreme than for the fast-cooled data; although the 111 and 222 peaks remained as sharp as previously, peaks with hkl, $h \neq k$, and hkl, $l = 0$ can best be described as diffuse (Figure 3c, d). The extreme broadening persisted down to the lowest measured temperature of 20 K and prevented meaningful structural refinements from being performed. The peak maxima remain in approximately the same positions as in the fast-cooled data, indicating that the anion

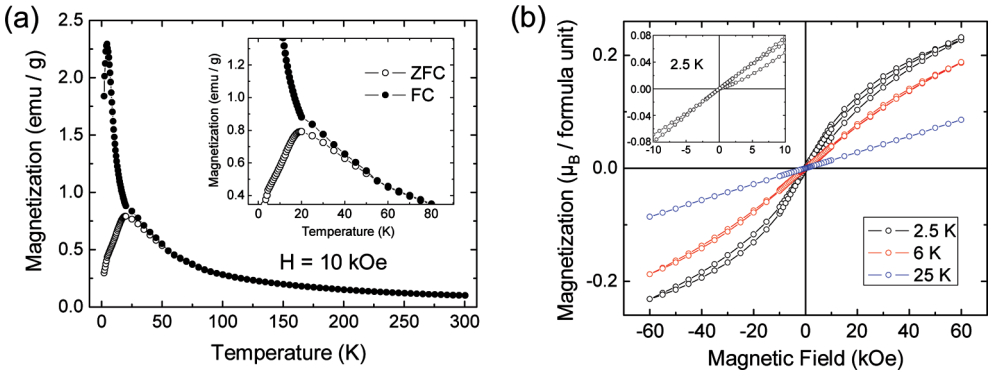

Figure 5. (a) ZFC and FC magnetization as a function of temperature. The inset shows an expanded view of the curves below 80 K. (b) Magnetization versus applied magnetic field at different temperatures. The inset shows an expanded view of the virgin curve at low field.

axes are still confined to the *ab* plane below the transition. Therefore, it appears that slow cooling rather surprisingly results in smaller structural domains in the *ab* plane. Subsequent XRD measurements revealed that the domain density is only influenced by the rate at which the sample is cooled through the phase transition; for example, the rate of cooling between 200 and 20 K is unimportant. Furthermore, an XRD pattern collected after holding a slow-cooled sample at 20 K for a further 12 h was unchanged, implying that the domain structure below the transition is "locked-in".

3.3. Magnetic Properties. All magnetic data discussed below were collected after fast cooling the sample from room temperature to the starting temperature of each given measurement (the ~50 K phase transition region was always crossed in less than 10 min). The sample was always warmed back to room temperature between successive measurements. Figure 5a shows the magnetization of $RbO_{1.72}$ as a function of temperature, measured on warming in a field of 10 kOe. The field-cooled (FC) and zero-field-cooled (ZFC) curves exhibit splitting below an irreversibility temperature of ~50 K; the splitting becomes more pronounced below 20 K. Larger applied fields of up to 50 kOe gave essentially identical susceptibility curves. Peaks are apparent at ~20 K in the ZFC curve and at ~5 K in the FC curve. The ZFC-FC irreversibility is typical of magnetically frustrated or disordered systems and can indicate a spin-glass in which individual spins interact strongly, a superparamagnet consisting of isolated clusters of FM-coupled spins, or the intermediate situation of a cluster glass with weak to moderate interactions between the FM clusters.[34−36] In the latter case, the ZFC peak at 20 K would correspond to the so-called blocking temperature T_f, below which the net moments in different clusters are frozen into a random configuration. This scenario is supported by further magnetic measurements described below. A fit to the temperature dependence of the inverse magnetic susceptibility in the paramagnetic region using a modified Curie−Weiss law ($\chi = C/(T - \theta) + \chi_0$) yielded an effective moment of 1.64 μ_B. The inclusion of a temperature-independent χ_0 term was necessary in order to obtain a linear temperature dependence of χ^{-1}. Considering that 86% of the anion sites are occupied, this value corresponds to an effective moment of 1.77 μ_B per anion, which is somewhat higher than the spin-only value expected for a $S = 1/2$ system (1.73 μ_B) considering that there are nominally only 0.84 spins on each anion. We note that spin−orbit coupling is significant for the superoxide anion and considerable unquenched orbital moments are thought to be present in the paramagnetic phases of stoichiometric AO_2,[18,20] often manifested by high values of μ_{eff}.[31,37] We obtained a Weiss constant (θ) of −3.4 K from our Curie−Weiss fit, which is small compared to the magnetic irreversibility temperature of 50 K and suggests that AFM and FM interactions compete. The presence of FM interactions is evidenced by measurements of magnetization as a function of applied magnetic field (Figure 5b). At 2.5 K, a narrow, pinched hysteresis loop opens at applied fields of above ~10 kOe, indicating a FM response. However, there is no remanence and saturation was not achieved up to 60 kOe, where a magnetization of ~0.25 μ_B/f.u. is reached. This corresponds to 35% of the nominal saturation of a FM magnetization. Holding the sample overnight in 60 kOe did not result in any further increase in magnetization. The shape of the 2.5 K $M-H$ curve is consistent with either an additional AFM component or with spins that remain disordered to low temperature. The peak in the FC magnetization at 5 K and the low value of θ suggest that the remaining spins order in AFM fashion. We note that at low fields, the virgin $M-H$ curve lies outside the hysteresis loop measured on subsequent cycling (see inset to Figure 5b), a feature previously observed for the cluster glass superconductor Ru1222[38] and magnetic Fe_2O_3 nanoparticles that act as a cluster glass.[39] At 6 K, the field-induced ferromagnetism is weaker; the hysteresis loop is narrower and opens only above ~15 kOe. A linear $M-H$ dependence with no hysteresis is apparent at 25 K.

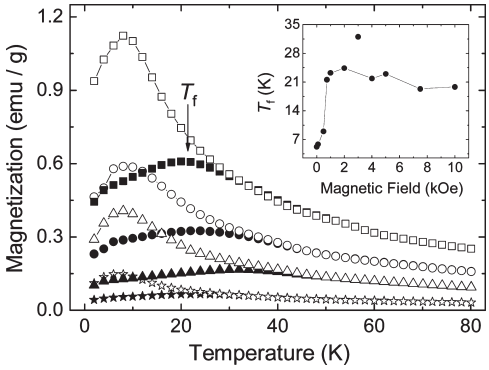

Figure 6. ZFC (open symbols) and FC (closed symbols) magnetization measured in applied fields of (from bottom to top) 1, 3, 5, and 7.5 kOe. The inset shows the variation in the ZFC peak temperature (T_f) with field.

Figure 6 shows the ZFC and FC magnetization of $RbO_{1.72}$ measured on warming in different applied fields. For a canonical spin glass, mean-field theory predicts that the peak in the ZFC

dx.doi.org/10.1021/cm103433r |*Chem. Mater.* 2011, 23, 1578–1586

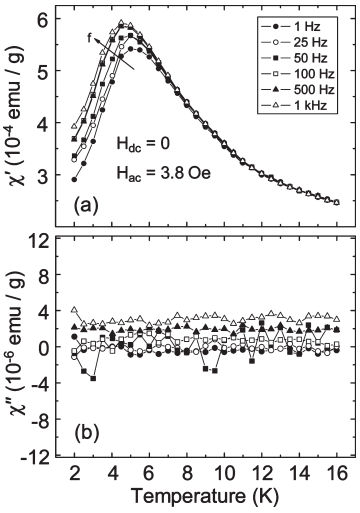

Figure 7. AC magnetic susceptibility as a function of temperature: (a) in-phase component; (b) out-of-phase component.

curve, which would correspond to the so-called spin freezing temperature, should vary with $H^{2/3}$.[40] This is clearly not the case for our sample (see inset to Figure 6), where T_f initially increases rapidly at low fields and then exhibits a gradual decrease above 3 kOe. However, this type of behavior has previously been observed in, for example, FM Fe_2O_3 and FePt nanoparticles and is instead consistent with the formation of spin clusters with a distribution of sizes.[41,42] The temperature required to "unblock" large clusters is higher than that required for small clusters; the maximum in the ZFC curve then has no particular physical meaning, being a superposition of contributions from larger blocked clusters and smaller deblocked clusters that behave in superparamagnetic fashion. The unusual dependence of T_f on field was explained for the above nanoparticle systems by considering how the distribution of magnetic anisotropy energy barriers and the magnetic relaxation above the blocking temperature vary with respect to particle size and field.[41,42]

AC susceptibility measurements, shown in Figure 7, provide more evidence against the presence of a canonical spin-glass state in $RbO_{1.72}$. The sample was cooled to 2 K in zero field before applying an AC field of 3.8 Oe in the absence of a DC field and measuring the susceptibility on warming. A peak in the in-phase susceptibility (χ') is observed at ~5 K; this is consistent with the field dependence of the DC ZFC magnetization peak (see Figure 6, inset). The peak in χ' shifts toward lower temperature with increasing frequency, opposite to the expected trend for a spin glass. Such behavior has previously been reported for the cluster glass system $NaNiO_2$[43] and signals the presence of multiple relaxation rates due to a distribution of cluster sizes. For canonical spin glasses, the strong interactions between spins would also result in spin lag (dissipation) manifested as a peak in the out-of-phase susceptibility (χ''), the maximum slope of which should coincide with the peak in χ'.[35] The absence of a measurable change in χ'' in our data is somewhat surprising, but the signal is close to the sensitivity limit of the magnetometer and a suppression of the χ'' peak is expected for spin clusters with a broad distribution of sizes and thus relaxation times.[36]

Further evidence for the formation of FM clusters was obtained from measurements of magnetization versus time in low fields. The sample was cooled from room temperature to 6 K at a rate of 5 K/min in zero field, where it was left for a certain

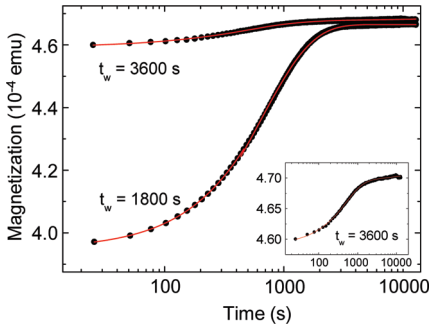

Figure 8. Magnetization as a function of time measured at 6 K in a field of 100 Oe after waiting for 1800 and 3600 s in zero field. The inset shows an expanded view of the t_w = 3600 s data.

Table 2. Fit Parameters (see eq 1) for the Time Dependence of Magnetization at 6 K Shown in Figure 8

t_w (s)	m_0 (emu)	m_1 (emu)	τ_0 (s)	α
1800 (t < 1000 s)	$3.9(1) \times 10^{-4}$	$9.0(1) \times 10^{-5}$	1120(20)	0
1800 (t > 1000 s)	$3.8(1) \times 10^{-4}$	$8.0(1) \times 10^{-5}$	634(2)	0
3600	$4.6(1) \times 10^{-4}$	$7.0(1) \times 10^{-6}$	511(6)	$-6.0(2) \times 10^{-4}$

"waiting time", t_w. A field of 100 Oe was then applied and the magnetization was measured as a function of time, as shown in Figure 8 for t_w = 1800 and 3600 s. It is clear that the spin dynamics are slow; the magnetization increases with time and reaches a plateau after 1−2 h. Application of a magnetic field likely rotates the anions within the FM clusters such that their associated magnetic moments become aligned closer to the field (the easy axis of magnetization is perpendicular to the anion axis in AO_2[23]). The cooperative rotation of superoxide anions in AO_2 is known to be a hindered process with a high energy barrier, similar to that in other molecular crystals such as the nonmagnetic alkali metal cyanides.[44] Therefore, the net moments of the clusters are only partially rotated in the fields accessed in our current study and a metastable state is reached corresponding to the magnetization plateau in Figure 8. The evolution of magnetization was fitted using the following function

$$M = m_0(t^{-\alpha}) + m_1(1 - \exp(-t/\tau_0)) \qquad (1)$$

The fitted parameters are shown in Table 2. For t_w = 3600 s the curve could be fitted well by the sum of exponential and power law terms in eq 1. In contrast, it was necessary to split the t_w = 1800 s curve into two parts (t < 1000 s and t > 1000 s), each of which could be fitted well using only the exponential term of eq 1. This implies that for t_w = 1800 s, two groups of clusters can be distinguished that respond to the field on two distinct time scales. When the sample is held for longer before applying a field, the net moments of the FM clusters are already aligned in a more FM fashion, as indicated by the higher initial magnetization for the t_w = 3600 s curve. This might be the result of a small residual field in the magnet.

An exponential-type magnetic response (measured as here after applying a field) or decay (measured after switching off an applied field) has previously been observed in both cluster glass and ferromagnetic nanoparticle systems,[38,45−47] as well as magnetically frustrated $RbO_{1.5}$ and $CsO_{1.5}$.[26] Monte Carlo simulations have suggested that the functional form of the slow response or decay below the blocking temperature depends on the concentration of magnetic clusters and on the strength of the

dx.doi.org/10.1021/cm103433r |Chem. Mater. 2011, 23, 1578–1586

interactions between them.[48] An exponential response is predicted for low cluster densities and hence weak interactions, whereas power-law behavior is predicted for higher densities where the interactions between clusters are strong, as well as for canonical spin glasses.[49] Our data suggest that an intermediate scenario is applicable to $RbO_{1.72}$, where moderately strong intercluster interactions are present. Above the blocking temperature $RbO_{1.72}$ acts more like a superparamagnet until the short-range FM order is lost at ~50 K, followed by normal paramagnetic behavior at higher temperature. The FM clusters probably exist in a matrix of AFM order that becomes long-range below ~5 K.

4. DISCUSSION

We have shown that $RbO_{1.72}$, unlike all other alkali metal oxides studied thus far, exhibits three-dimensional FM ordering (within clusters). Furthermore, the temperature at which the FM clusters begin to form (~50 K) is significantly higher than the AFM ordering temperatures of AO_2 and $AO_{1.5}$ (A = Rb, Cs).[26,50] The three-dimensional FM exchange in $RbO_{1.72}$ must be a consequence of the oxygen nonstoichiometry, which leads to a situation in which the π_g orbitals nominally contain a nonintegral number of electrons. Two scenarios are then possible. First, a true mixed-valent situation may arise in which the π_g electrons are itinerant, hopping between adjacent anions. Second, the π_g electrons may be localized, in which case there will be a tendency to remove the orbital degeneracy and split the energies of the π_x and π_y orbitals by means of a structural distortion. Both types of systems are well-known in transition metal oxides that possess partially filled e_g orbitals, typified by the doped rare-earth manganite perovskites $R_{1-x}AE_xMnO_3$ (R = rare earth, AE = alkaline earth), which are famous for their colossal magnetoresistance properties.[24] At low doping levels insulating phases are always found, and a Jahn−Teller distortion takes place at which spatial ordering of the occupied e_g orbitals sets in. In most cases this OO gives rise to AFM superexchange, although OO, FM insulating phases are sometimes found, for example at $0.1 < x < 0.2$ in $La_{1-x}Ca_xMnO_3$.[51] As the trivalent R^{3+} is progressively replaced by divalent AE^{2+}, Mn^{3+} is nominally replaced by Mn^{4+}. The Jahn−Teller distortion associated with the orbitally degenerate Mn^{3+} cation is suppressed above a critical doping level.[51,52] Electrons can then hop dynamically between the e_g levels of adjacent Mn^{3+} and Mn^{4+} cations, a process known as double exchange, which gives rise to FM metallic behavior. Although no metallic AO_{2-x} compound has yet been discovered, double exchange is a possible explanation for the FM clusters that we observe in $RbO_{1.72}$. This scenario would likely involve droplets of non-OO anions embedded in an AFM/OO matrix, which is a type of inhomogeneity widely observed in the doped manganites.[24,53] Alternatively, it is also possible that FM exchange might arise within an OO phase, as discussed below.

We now discuss the structural properties of $RbO_{1.72}$ in the context of possible OO configurations and their relationship with magnetic exchange interactions. In the cubic symmetry of the room-temperature phase, the π_g orbitals are 2-fold degenerate.[50] On cooling through the transition at 230 K, the anions become orientationally ordered in the *ab* plane, accompanied by small shifts of their centers of mass along the two [110] directions and a consequent reduction of the crystal symmetry. The probable driving force behind this anion ordering transition is to split the π_g orbitals in energy and thus lift the degeneracy, as occurs in

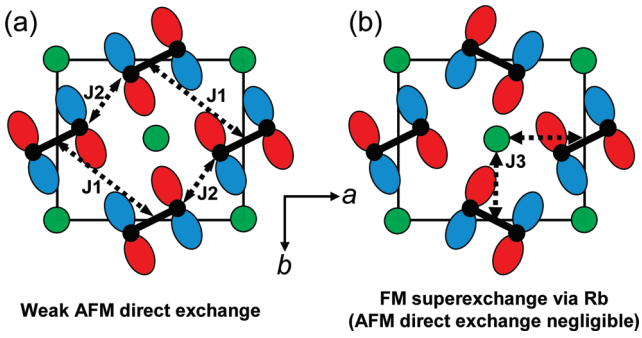

Figure 9. Possible "ferro" ordering of half-filled antibonding π-orbitals in the *ab*-plane for domains in which anions are rotated in the (a) same and (b) opposite directions. The Rb^+ cations are represented by green circles.

stoichiometric AO_2.[16,18,50] This is similar to the Jahn−Teller effect in transition metal oxides, which involves displacement of the ligands surrounding the orbitally degenerate cation, but with the difference that the rotational degrees of freedom of the dioxygen anion provide an extra degree of flexibility as to how such a symmetry lowering transition can take place. We thus expect that orbital ordering (OO) is present below 230 K in $RbO_{1.72}$, although our powder XRD data do not allow us to determine its nature due to the small size of the structural domains.

A series of recent theoretical studies on stoichiometric AO_2 suggest that the spin, orbital and lattice degrees of freedom in dioxygen anion systems are intimately connected,[18−22] as is commonly the case in transition metal oxides. The best studied member of the series is KO_2, which adopts a magnetic structure thought to consist of FM planes that are coupled in AFM fashion.[54] Calculations have suggested that at low temperature the lobes of half-filled π orbitals on adjacent anions point toward each other in the *ab* plane, a "ferro" OO state.[18,20] Although this geometry promotes AFM direct exchange,[50,55] it has been proposed that superexchange via the cations is also significant in KO_2; this has been calculated to tip the balance in favor of FM interactions within the plane.[20]

It is likely that the vacancies on the dioxygen sublattice in $RbO_{1.72}$ lower the energy barrier to anion rotation with respect to that in stoichiometric RbO_2, allowing lifting of the orbital degeneracy by the adoption of a different crystal structure. Looking at the *ab* plane of low-temperature $RbO_{1.72}$, two local structural configurations can be envisaged; nearest-neighbor (NN) anions can be rotated in the same or opposite directions to give parallel or staggered patterns. In domains adopting the former configuration, assuming the simplest case of "ferro" OO in which the lobes of the half-occupied antibonding π-orbitals also lie in the *ab* plane, a degree of direct orbital overlap is possible, giving small AFM coupling constants J1 and J2 (Figure 9a). The anion tilt angle of ~20° prevents strong orbital overlap in any configuration and is consistent with the low ordering temperature of ~5 K of the AFM component of the sample (Figure 5a). In the staggered anion arrangement in Figure 9b no significant orbital overlap between NN anions will occur and no significant in-plane AFM exchange is possible. No appreciable interplane NN orbital overlap would occur for either anion configuration. However, if the unoccupied 4d-states of Rb are accessible in terms of energy, three-dimensional FM superexchange via Rb might dominate for the staggered configuration (J3 in Figure 9b indicates a NN superexchange pathway within the *ab* plane). The FM clusters

that we observe experimentally might be comprised of domains with the staggered anion arrangement, an alternative to the double-exchange scenario described above. We note that the coexistence of domains with different OO configurations is known in polycrystalline samples of transition metal oxides, as we have previously demonstrated for RVO_3 perovskites.[56,57]

Finally, we mention briefly that preliminary measurements of magnetization versus temperature and field on a sample of $RbO_{1.72}$ that was slow-cooled through the phase transition indicated AFM ordering below ~5 K, with none of the signals of FM ordering or cluster glass behavior observed for fast cooling (see the Supporting Information). It thus appears that slow cooling suppresses formation of the FM domains (whether orbitally ordered or not) that are formed on fast cooling; these might be associated with a metastable structural state. It is evident that the local structure of $RbO_{1.72}$ should be examined in order to gain more insight into the anion configurations that exist within domains, and calculations are necessary in order to confirm whether FM superexchange is feasible or whether double exchange is more likely. Furthermore, we cannot neglect the influence on the magnetic properties of domain boundaries between structurally coherent regions (the density of which also depends on the cooling rate), and of grain boundaries in the polycrystalline sample.

5. CONCLUSION

We have studied the effect of oxygen deficiency on the properties of AFM RbO_2. A novel phase with composition $RbO_{1.72}$ can be stabilized by heating RbO_2 in vacuum. Below ~230 K the orientationally disordered anions become ordered in a plane and the orbital degeneracy of the superoxide anion is lifted. The low-temperature structure is comprised of orbitally ordered nanodomains, the density of which depends on the cooling rate through the transition. Short-range FM ordering sets in at ~50 K in the form of clusters; a FM cluster-glass state is formed below a blocking temperature of ~20 K, embedded in an AFM matrix that orders at ~5 K. The nonspherical nature of the dioxygen anions in AO_{2-x} plays an important role in the interplay between the spin, orbital and lattice degrees of freedom. We have studied the effect of another parameter, nonstoichiometry, and have shown that it can generate strong FM interactions, in contrast to the AFM interactions conventionally present in stoichiometric AO_2. We have thus demonstrated a new mechanism to induce ferromagnetism in p-electron systems.

■ ASSOCIATED CONTENT

Supporting Information. Zero-field-cooled magnetic susceptibilities for fast and slow-cooled samples. X-ray crystallographic information file (CIF) for $RbO_{1.72}$ at 20 K. This material is available free of charge via the Internet at http://pubs.acs.org.

■ AUTHOR INFORMATION

Corresponding Author
*E-mail: g.r.blake@rug.nl.

■ ACKNOWLEDGMENT

This work is supported by a VIDI fellowship from the Dutch National Science Organization (NWO).

■ REFERENCES

(1) Son, Y. -W.; Cohen, M. L.; Louie, S. G. *Nature* **2006**, *444*, 347–349.
(2) Tombros, N.; Jozsa, C.; Popinciuc, M.; Jonkman, H. T.; van Wees, B. J. *Nature* **2007**, *448*, 571–574.
(3) Coey, J. M. D. *Curr. Opin. Solid State Mater. Sci.* **2006**, *10*, 83–92.
(4) Sundaresan, A.; Rao, C. N. R. *Nano Today* **2009**, *4*, 96–106.
(5) Volnianska, O.; Boguslawski, P. *J. Phys.: Condens. Matter* **2010**, *22*, 073202.
(6) Freiman, Yu. A.; Jodl, H. J. *Phys. Reports* **2004**, *401*, 1–228.
(7) Meier, R. J.; Helmholdt, R. B. *Phys. Rev. B* **1984**, *29*, 1387–1393.
(8) Klotz, S.; Strässle, Th.; Cornelius, A. H.; Philippe, J.; Hansen, Th. *Phys. Rev. Lett.* **2010**, *104*, 115501.
(9) van Hemert, M. C.; Wormer, P. E. S.; van der Avoird, A. *Phys. Rev. Lett.* **1983**, *51*, 1167–1170.
(10) Bussery, B.; Wormer, P. E. S. *J. Chem. Phys.* **1993**, *99*, 1230–1239.
(11) Hanami, K.; Umesaki, T.; Matsuda, K.; Miyata, Y.; Kataura, H.; Okabe, Y.; Maniwa, Y. *J. Phys. Soc. Jpn.* **2010**, *79*, 023601.
(12) Kawakami, T.; Takamizawa, S.; Takenaka, M.; Nishimura, Y.; Kitagawa, Y.; Okumura, M.; Mori, W.; Yamaguchi, K. *Polyhedron* **2007**, *26*, 2367–2374.
(13) Takamizawa, S.; Nakata, E.; Akatsuka, T.; Kachi-Terajima, C.; Miyake, R. *J. Am. Chem. Soc.* **2008**, *130*, 17882–17892.
(14) Attema, J. J.; de Wijs, G. A.; Blake, G. R.; de Groot, R. A. *J. Am. Chem. Soc.* **2005**, *127*, 16325–16328.
(15) Hesse, W.; Jansen, M.; Schnick, W. *Prog. Solid State Chem.* **1989**, 47–110.
(16) Halverson, F. *J. Phys. Chem. Solids* **1962**, *23*, 207–214.
(17) Kemeny, G.; Kaplan, T. A.; Mahanti, S. D.; Sahu, D. *Phys. Rev. B* **1981**, *24*, 5222–5228.
(18) Solovyev, I. V. *New J. Phys.* **2008**, *10*, 013035.
(19) Kováčik, R.; Ederer, C. *Phys. Rev. B* **2009**, *80*, 140411.
(20) Kim, M.; Kim, B. H.; Choi, H. C.; Min, B. I. *Phys. Rev. B* **2010**, *81*, 100409.
(21) Ylvisaker, E. R.; Singh, R. R. P.; Pickett, W. E. *Phys. Rev. B* **2010**, *81*, 180405.
(22) Nandy, A. K.; Mahadevan, P.; Sen, P.; Sarma, D. D. *Phys. Rev. Lett.* **2010**, *105*, 056403.
(23) Labhart, M.; Raoux, D.; Känzig, W.; Bösch, M. A. *Phys. Rev. B* **1979**, *20*, 53–70.
(24) Dagotto, E. *New J. Phys.* **2005**, *7*, 67.
(25) Winterlik, J.; Fecher, G. H.; Jenkins, C. A.; Felser, C.; Mühle, C.; Doll, K.; Jansen, M.; Sandratskii, L. M.; Kübler, J. *Phys. Rev. Lett.* **2009**, *102*, 016401.
(26) Winterlik, J.; Fecher, G. H.; Jenkins, C. A.; Medvedev, S.; Felser, C.; Kübler, J.; Mühle, C.; Doll, K.; Jansen, M.; Palasyuk, T.; Trojan, I.; Eremets, M. I.; Emmerling, F. *Phys Rev. B* **2009**, *79*, 214410.
(27) Larson, A. C.; Von Dreele, R. B. *Los Alamos National Laboratory LAUR Report* 2004, *No.* 86-748.
(28) Toby, B. H. *J. Appl. Crystallogr.* **2001**, *34*, 210–213.
(29) Cheary, R. W.; Coelho, A. A. *Programs XFIT and FOURYA, deposited in CCP14 Powder Diffraction Library*; Engineering and Physical Sciences Research Council, Daresbury Laboratory: Warrington, England (http://www.ccp14.ac.uk/tutorial/xfit-95/xfit.htm)
(30) Eysel, H. H.; Thym, S. *Z. Anorg. Allg. Chem.* **1975**, *411*, 97–102.
(31) Känzig, W.; Labhart, M. *J. Physique Coll.* **1976**, *37* (C7), 39–45.
(32) Dietzel, P. D. C.; Kremer, R. K.; Jansen, M. *Chem. Asian J.* **2007**, *2*, 66–75.
(33) Stephens, P. *J. Appl. Crystallogr.* **1999**, *32*, 281–289.
(34) Mamiya, H.; Nimori, S.; Ohnuma, M.; Nakatani, I.; Demura, M.; Furubayashi, T. *J. Magn. Magn. Mater.* **2007**, *316*, e535–e537.
(35) Mydosh, J. A. *Spin Glasses: An Experimental Introduction*; Taylor & Francis: London, 1993.
(36) Bedanta, S.; Kleemann, W. *J. Phys. D: Appl. Phys.* **2009**, *42*, 013001.

(37) Dietzel, P. D. C.; Kremer, R. K.; Jansen, M. *J. Am. Chem. Soc.* **2004**, *126*, 4689–4696.
(38) Cardoso, C. A.; Araujo-Moreira, F. M.; Awana, V. P. S.; Takayama-Muromachi, E.; de Lima, O. F.; Yamauchi, H.; Karppinen, M. *Phys. Rev. B* **2003**, *67*, 020407.
(39) Zysler, R. D.; Fiorani, D.; Testa, A. M. *J. Magn. Magn. Mater.* **2001**, *224*, 5–11.
(40) de Almeida, J. R. L.; Thouless, D. J. *J. Phys. A* **1978**, *11*, 983–990.
(41) Sappey, R.; Vincent, E.; Hadacek, N.; Chaput, F.; Boilot, J. P.; Zins, D. *Phys. Rev. B* **1997**, *56*, 14551–14559.
(42) Zheng, R. K.; Gu, H.; Xu, B.; Zhang, X. X. *J. Phys.: Condens. Matter* **2006**, *18*, 5905–5910.
(43) Baker, P. J.; Lancaster, T.; Blundell, S. J.; Brooks, M. L.; Hayes, W.; Prabharakaran, D.; Pratt, F. L. *Phys. Rev. B* **2005**, *72*, 104414.
(44) Lynden-Bell, R. M.; Michel, K. H. *Rev. Mod. Phys.* **1994**, *66*, 721–762.
(45) Li, D. X.; Nimori, S.; Shiokawa, Y.; Haga, Y.; Yamamoto, E.; Onuki, Y. *Phys. Rev. B* **2003**, *68*, 172405.
(46) Thakur, M.; Patra, M.; Majumdar, S.; Giri, S. *J. Appl. Phys.* **2009**, *105*, 073905.
(47) Mukadam, M. D.; Yusuf, S. M.; Sharma, P.; Kulshreshtha, S. K.; Dey, G. K. *Phys. Rev. B* **2005**, *72*, 174408.
(48) Ulrich, M.; García-Otero, J.; Rivas, J.; Bunde, A. *Phys. Rev. B* **2003**, *67*, 024416.
(49) Binder, K.; Young, A. P. *Rev. Mod. Phys.* **1986**, *58*, 801–976.
(50) Mahanti, S. D.; Kemeny, G. *Phys. Rev. B* **1979**, *20*, 2105–2117.
(51) van Aken, B. B.; Jurchescu, O. D.; Meetsma, A.; Tomioka, Y.; Tokura, Y.; Palstra, T. T. M. *Phys. Rev. Lett.* **2003**, *90*, 066403.
(52) Božin, E. S.; Schmidt, M.; DeConinck, A. J.; Paglia, G.; Mitchell, J. F.; Chatterji, T.; Radaelli, P. G.; Proffen, Th.; Billinge, S. J. L. *Phys. Rev. Lett.* **2007**, *98*, 137203.
(53) Mathieu, R.; Tokura, Y. *J. Phys. Soc. Jpn.* **2007**, *76*, 124706.
(54) Smith, H. G.; Nicklow, R. M.; Raubenheimer, L. J.; Wilkinson, M. K. *J. Appl. Phys.* **1966**, *37*, 1047–1049.
(55) Kugel, K. I.; Khomskii, D. I. *Sov. Phys. Usp.* **1982**, *25*, 231–256.
(56) Sage, M. H.; Blake, G. R.; Nieuwenhuys, G. J.; Palstra, T. T. M. *Phys. Rev. Lett.* **2006**, *96*, 036401.
(57) Sage, M. H.; Blake, G. R.; Marquina, C.; Palstra, T. T. M. *Phys. Rev. B* **2007**, *76*, 195102.